View metadata, citation and similar papers at core.ac.uk
brought to you by CORE
provided by Aston Publications Explorer

Fiber Bragg gratings inscribed using 800nm femtosecond laser and a phase mask in single- and multi-core mid-IR glass fibers

Rui Suo,[1,*] Joris Lousteau,[2] Hongxia Li,[3] Xin Jiang,[2] Kaiming Zhou,[1] Lin Zhang,[1] William N MacPherson,[3] Henry T Bookey,[3] James S Barton[3], Ajoy K Kar,[3] Animesh Jha[2] and Ian Bennion[1]

[1]*Photonics Research Group, Aston University, Birmingham, UK, B47ET*
[2]*Institute for Materials Research, University of Leeds, Clarendon Road, Leeds LS2 9JT, UK*
[3]*Department of Physics, School of Engineering and Physical Sciences, Heriot-Watt University, Edinburgh EH14 4AS, UK*
**Corresponding author: suor@aston.ac.uk*

Abstract: For the first time, Fiber Bragg grating (FBG) structures have been inscribed in single-core passive germanate and three-core passive and active tellurite glass fibers using 800nm femtosecond (*fs*) laser and phase mask technique. With *fs* peak power intensity in the order of 10^{11}W/cm^2, the FBG spectra with 2nd and 3rd order resonances at 1540 and 1033nm in the germanate glass fiber and 2nd order resonances at ~1694 and ~1677nm with strengths up to 14dB in all three cores in the tellurite fiber were observed. Thermal responsivities of the FBGs made in these mid-IR glass fibers were characterized, showing average temperature responsivity ~20pm/°C. Strain responsivities of the FBGs in germanate glass fiber were measured to be 1.219pm/με.

©2009 Optical Society of America

OCIS codes: (320.7140) Ultrafast process in fibers; (060.3735) Fiber Bragg gratings.

References and links

1. S. Shen, A. Jha, X. Liu, M. Naftaly, K. Bindra, H. J. Bookey, and A. K. Kar, "Tellurite glasses for broadband amplifiers and integrated optics," J. Am. Ceram. Soc. **85**, 1391-1395 (2002).
2. T. Uemura, K. Nishida, M. Sakakida, K. Ichinose, S. Shimoda, and M. Shichiri, "Non-invasive blood glucose measurement by Fourier transform infrared spectroscopic analysis through the mucous membrane of the lip: application of a chalcogenide optical fiber system," Frontiers Med. Biol. Eng. **9**, 137-153 (1999).
3. J. Mulrooney, J. Clifford, C. Fitzpatrick, and E. Lewis, "Detection of carbon dioxide emissions from a diesel engine using a mid-infrared optical fibre based sensor," Sens. Actuators A: Physical. **136**, 104-110 (2007).
4. K. S. Bindra, H. T. Bookey, A. K. Kar, B. S. Wherrett, X. Liu, and A. Jha, "Nonlinear optical properties of chalcogenide glasses: Observaton of multiphoton absorption," Appl. Phys. Lett. **79**, 1939-1941(2001).
5. A. Mori, H. Masuda, K. Shikano, and M. Shimizu, "Ultra-wide-band tellurite-based fiber Raman amplifier." J. Lightwave Technol. **21**, 1300-13106 (2003).
6. A. Céreyon, B. Champagnon, V. Martinez, L. Maksimov, O. Yanush, and V. N. Bogdanov, "xPbO-(1-x)GeO2 glasses as potential materials for Raman amplification," Opt. Mater. **28**, 1301-1304 (2006).
7. M. Silva-López, W. N. MacPherson, C. Li, A. J. Moore, J. S. Barton, J. D. C. Jones, D. Zhao, L. Zhang, and I. Bennion, "Transverse load and orientation measurement with multicore fiber Bragg gratings," Appl. Opt. **44**, 6890-6897 (2005).
8. G. M. H. Flockhart, W. N. MacPherson, J. S. Barton, J. D. C. Jones, L. Zhang, and I. Bennion, "Two-axis bend measurement with Bragg gratings in multicore optical fiber," Opt. Lett. **28**, 387-389 (2003).
9. P. Glas, M. Naumann, A. Schirmacher, and Th. Pertsch, "The multicore fiber - a novel design for a diode pumped fiber laser." Opt. Commun. **151**, 187-195 (1998).
10. X. Jiang, J. Lousteau, and A. Jha, "Raw materials purification for the development of high performance infrared transmitting germanate glass fibre," Glass Technology: The European Journal of Glass Science & Technology, Part A in press (2008)
11. J. Lousteau, H. Bookey, X. Jiang, C. Hill, A. Kar, and A. Jha, "Fabrication of multicore tellurite glass optical fibres," in Proceedings of IEEE International Conference on Transparent Optical Networks (Institute of Electrical and Electronics Engineers, Rome, 504-509, (2007).

#108667 - $15.00 USD Received 11 Mar 2009; revised 9 Apr 2009; accepted 15 Apr 2009; published 22 Apr 2009
(C) 2009 OSA

12. H. T. Bookey, J. Lousteau, A. Jha, N. Gayraud, R. R. Thomson, N. D. Psaila, H. Li, W. N. MacPherson, J. S. Barton, and A. K. Kar, "Multiple rare earth emissions in a multicore tellurite fiber with a single pump wavelength," Opt. Express. **15**, 17554-17561 (2007).
13. S. J. Mihailov, C. W. Smelser, D. Grobnic, R. B.Walker, P. Lu, H. Ding, and J. Unruh, "Bragg gratings written in all-SiO_2 and Ge-doped core fibers with 800-nm femtosecond radiation and a phase mask," J. Lightwave Technol. **22**, 94-100 (2004).
14. C. W. Smelser, S. J. Mihailov, D. Grobnic, P. Lu, R. B.Walker, H. Ding, and X. Dai, "Multiple-beam interference patterns in optical fiber generated with ultrafast pulses and a phase mask," Opt. Lett. **29**, 1458-1460 (2004).
15. C. W. Smelser, D. Grobnic, and S. J. Mihailov, "Generation of pure two-beam interference grating structures in an optical fiber with a femtosecond infrared source and a phase mask," Opt. Lett. **29**, 1730-1732 (2004).
16. C. W. Smelser, S. J. Mihailov, and D. Grobnic, "Rouard's method modeling of type I-IR fiber Bragg gratings made using an ultrafast IR laser and a phase mask," J. Opt. Soc. Am. B. **23**, 2011-2017 (2006).
17. C. W. Smelser, S. J. Mihailov, and D. Grobnic, "Impact of index change saturation on the growth behavior of higher-order type I ultrafast induced fiber Bragg gratings," J. Opt. Soc. Am. B. **25**, 877-883 (2008).
18. C. W. Smelser, S. J. Mihailov, and D. Grobnic, "Formation of Type I-IR and Type II-IR gratings with an ultrafast IR laser and a phase mask", Opt. Express. **13**, 5377-5386 (2005).
19. N. M. Dragomir, C. Rollinson, S. A.Wade, A. J. Stevenson, S. F. Collins, G. W. Baxter, P. M. Farrell, and A. Roberts, "Nondestructive imaging of a type I optical fiber Bragg grating," Opt. Lett. **28**, 789–791 (2003).
20. X. Shu, K. Sugden, D. Zhao, F. Floreani, L. Zhang and I. Bennion, "Complex growth behaviour of hybrid-type fibre Bragg gratings," Electron. Lett. **39**, 274-276 (2003).
21. S. S. Bayya, G. D. Chin, J. S. Sanghera, and I. D. Aggarwal, "Germanate glass as a window for high energy laser systems," Opt. Express **14**, 11687-11693 (2006).
22. H. Li, J. Lousteau, W. N. MacPherson, X. Jiang, H. T. Bookey, J. S. Barton, A. Jha, and A. K. Kar, "Thermal sensitivity of tellurite and germinate optical fibers," Opt.Express. **15**, 8857-8863 (2007).
23. A. I. Rabukhin, "Concentration dependences of elastooptic coefficients of germanate glasses containing lead and bismuth oxides," Glass and Ceramics. **37**, 87-90 (1995).
24. A. K. Ghatak and K. Thyagarajan, *Optical Electronics.* (Cambridge University Press), Chap.16, 1989, p503
25. A. EL-Adawy and R. EL-Mallawany, "Elastic modulus of tellurite glasses," J. Mater. Sci. Lett. **15**, 2065-2067 (1996).

1. Introduction

Germanate and tellurite glass fibers have attracted considerable attention to be explored for fiber devices in near and mid-IR regions. Their high refractive index and optical nonlinearity, resistance to corrosion, low melting temperature and good transmission properties from the visible to mid-IR region (0.35-6μm) [1] make them promising fiber hosts for bio/chemical and gas sensing [2-3], nonlinear optical signal processing [4] and optical amplifier and laser [5-6] devices. In recent years, we have also seen that there are increasingly reports for multi-core fibers (MCFs). MCFs can offer new device designs such as arrayed fiber sensors for load and bend measurement with direction recognition and temperature compensation capability [7-8] and arrayed fiber lasers and amplifiers which can scale up output powers [9]. Very recently, germanate and tellurite glass fibers with single- and three-core have been fabricated [10-11], and more significantly, the three-core tellurite glass fiber has been actively doped with $Ho^{3+}/Tm^{3+}/Yb^{3+}$, Er^{3+}/Ce^{3+}, and Tm^{3+}/Yb^{3+} respectively in each core and the emissions from the visible to mid-IR have been observed [12].

Single- and multi-core passive and active germanate and tellurite glass fibers represent a new class fiber host for devices which will extend photonics applications to mid-IR range, which is in increasing demands. Fiber Bragg grating (FBG) structures have been proven as one of the most functional in-fiber devices and vastly produced in silicate fibers by UV-inscription for countless laser and sensor applications. However, because germanate and tellurite fibers absorb UV greatly, FBG structures cannot be produced in such fibers by UV-inscription. In recent years, femtosecond (*fs*) lasers have been developed for laser machining and microstructuring in a variety of glass fibers and planar substrates. A number of papers have been reported on fabrication of FBGs and long-period gratings in optical fibers and also on the photosensitivity mechanism using 800 nm *fs* lasers [13-18].

#108667 - $15.00 USD Received 11 Mar 2009; revised 9 Apr 2009; accepted 15 Apr 2009; published 22 Apr 2009
(C) 2009 OSA

In this paper, we demonstrate for the first time the fabrication of FBGs in single-core passive germanate and three-core passive and active tellurite glass fibers by 800 nm *fs*-inscription. Using a 1697.33 nm period phase mask, the 2nd order FBG resonances with strength up to ~14 dB have been achieved in these mid-IR fibers and their thermal and strain responsivities have been characterized.

2. Fabrication and characteristics of germanate and tellurite glass fibers

The used germanate and tellurite fibers were drawn from glass compositions (mol%): $55GeO_2$-$30PbO$-$11Na_2O$-$4Ga_2O_3$ (GPNG) and $79TeO_2$-$14ZnO$-$7Na_2O$ (TZN), respectively for passive fibers, whereas for the active fiber the composition was $80TeO_2$-$10ZnO$-$10Na_2O$. The methods for fiber fabrication are described elsewhere [10-11]. The GPNG fiber has an undoped single-core with a diameter of ~8 μm surrounded by a cladding of ~126 μm diameter. The refractive indices of the core and cladding are 1.8622 and 1.8505 at 633 nm, respectively. The passive TZN fiber has three cores with diameters of ~12 μm and arranged equilaterally from the center with a separation of ~35 μm between each core, and surrounded by a cladding of ~130 μm diameter. The refractive indices of the TZN fiber core and cladding are measured as 2.0475 and 2.0224 at 633 nm, respectively. The active three-core TZN fiber has a similar form to the passive one, but with smaller core diameters, ~6 μm, and all three cores were doped with Er^{3+}/Ce^{3+}. However, it has a double-clad structure with the inner and outer cladding diameters of ~68 and ~120 μm with refractive indices of 2.0224 and ~1.9900 at 633 nm, respectively. The cross section images of the single-core GPNG and three-core passive and active TZN fibers are shown in Figs. 1(a)-1(c). Both GPNG and TZN fibers have much lower softening point for glass fabrication at approximately 480 °C and 320 °C, respectively, which are substantially lower than that (~1200 °C) of silica glass.

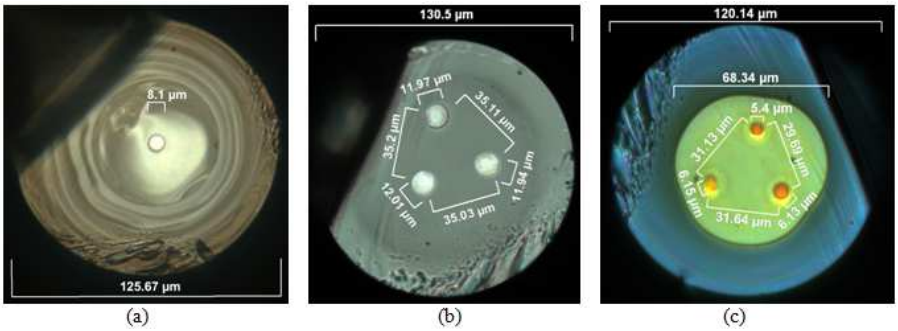

(a) (b) (c)

Fig. 1. Microscopy images of the cross-sections of (a) GPNG single-core fiber, (b) TZN passive and (c) active three-core fibers. Note: the D-shape-like end images are attributed to cleaving defects, as the fibres are not standard and fragile to achieve nice-finish cleaving.

3. FBG structures inscribed using femtosecond laser and phase mask

The FBG structures were produced in the GPNG and TZN fibers using *fs*-inscription through a custom-designed phase mask with a period of 1697.33 nm. Because of high refractive indices of the GPNG and TZN fibers, the phase mask was aiming to *fs*-inscribing 2nd order FBGs around 1500-1800 nm. The 800 nm *fs* laser power was from an amplified Ti:sapphire system with a repetition rate of 1kHz and a maximum output energy of ~1 mJ. The pulse duration measured by an autocorrelator was <120 *fs*. The output beam with a radius of 5 mm was focused in y-axis by a cylindrical lens of 30 mm focal length and through the phase mask to the fiber core. Due to the focusing effect of the high refractive index of the cladding, the laser beam was highly focused. Hence the width of *fs*-inscribed grating structure along *x*-axis, as shown in Fig. 2(b), is merely ~2 μm. Such a thin-layer of FBG structure would not give a high reflectivity and also in the experiment it was easy to miss the core region. To ensure maximum coverage of *fs*-inscription in the core region, the incident beam was scanned along the *x*-axis from -30 to 30 μm with an incremental step of 2 μm for the single-core GPNG fiber

#108667 - $15.00 USD Received 11 Mar 2009; revised 9 Apr 2009; accepted 15 Apr 2009; published 22 Apr 2009
(C) 2009 OSA

and from -50 to 50 μm for the three-core TZN fibers. After each shift, the translation stage was paused for 3 min letting the *fs*-exposing the focused fibre position. In order to eliminate the phase error which might be induced by the multi-scan along x-axis, the fibre was placed very close to the phase mask in the y-axis direction. It was noted that the *fs* power level is critical for inscribing FBG structure in the core without burning the fiber. Via systematical tests, we identified critical *fs* energy levels of ~22 and ~14 μJ to be suitable for inscribing FBGs in the GPNG and TZN fibers.

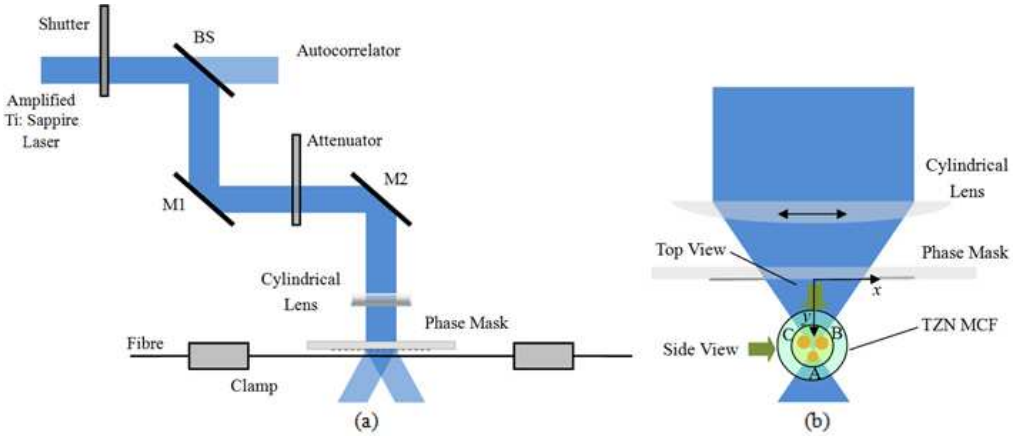

Fig. 2. Schematic diagram of FBG inscription system using *fs* laser and phase mask with a TZN MCF mounted. The *x* axis in (b) is parallel to the phase mask and perpendicular to the grooves; and the *y* axis is normal to the phase mask.

After *fs*-inscription, we first examined the FBG fringe structures under the microscope. For all inscribed GPNG and TZN fiber samples, we have seen clear fringe structures. Fig. 3(a) shows the top view (from the laser incident direction) image of an inscribed three-core TZN fiber and we can see all the three cores are fully covered by the continuous fringes. It is noted that, the different sizes of the imaged cores are due to different focus position of the microscope. Fig. 3(b) exhibits the side view image, the grating structure covering the almost the whole section depicts a typical three beams interference pattern. We measured the fringe space from the microscope image is 1.687 μm, which is close to the phase mask period, instead of a half of it. This is attributed to the Talbot effect [19] induced by the group-velocity walk-off of phase mask order pairs [14].

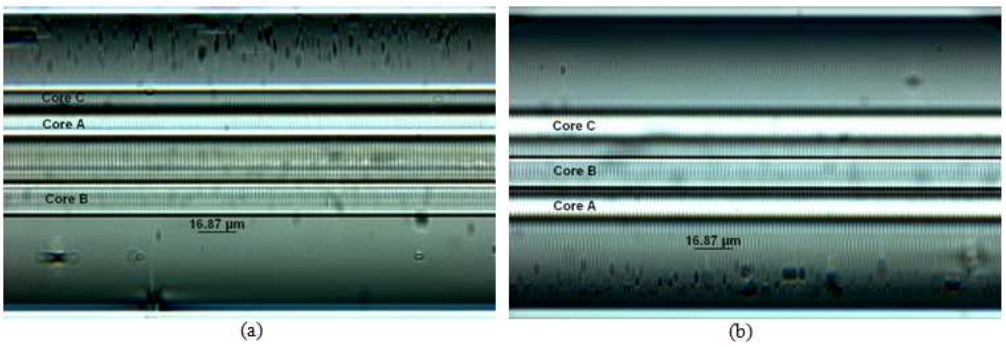

Fig. 3. Microscopy images of grating structure from (a) the top view and (b) side view of the TZN passive fiber. In both (a) and (b), the periods of the structures are measured as 1.687 μm.

4. Transmission properties

A super continuum broadband light source from Koheras with the output wavelength up to 1800nm was employed to examine the grating spectra of the fabricated FBGs in single-core

#108667 - $15.00 USD Received 11 Mar 2009; revised 9 Apr 2009; accepted 15 Apr 2009; published 22 Apr 2009
(C) 2009 OSA

GPNG and three-core TZN fibers using butt-coupling method. In order to ensure the light can be coupled into the individual cores of the three-core TZN fibers, we first examined the near-field patterns from the output end of the fiber for different coupling positions. Figures 4(a)-4(e) are the near-field images captured by an IR camera when the light was coupled into the outer cladding, inner cladding and the three individual cores, respectively. When in the near-field the cores were seen clearly, as shown for example in Figs. 4(c)-4(e), the output signal was then butt-coupled using a fiber lead to an optical spectrum analyzer to view FBG spectrum. Following this procedure, the spectra of all FBGs made in GPNG and TZN fibers were fully characterized.

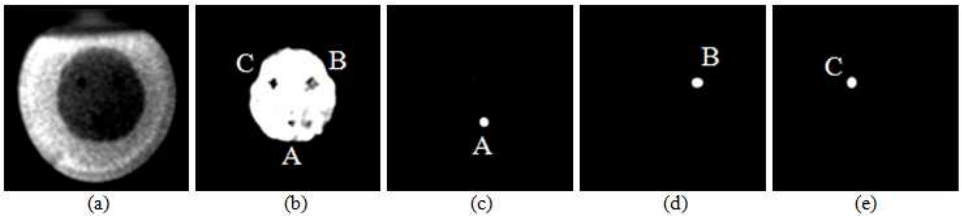

Fig. 4. Near-field patterns of a three-core TZN fiber when ~1680 nm light was launched into (a) outer cladding, (b) inner cladding, and (c) - (e) its three individual cores.

Figure 5(a) shows the 2nd order Bragg resonance of the GPNG fiber at 1540.42 nm with the strength of 6.5 dB. We also observed a very weak 3rd order resonance at 1033.74 nm with the strength of only 1.2 dB, as shown in Fig. 5(b). From the wavelengths of these two resonances, we calculated the refractive indices of the GPNG fiber as ~1.8156 and ~1.8271 at 1540 and 1034 nm, respectively. It is noted that the overall transmission losses in Figs. 5-7 are about 6-12dB, which are mainly attributed to the butt-coupling, as GPNG and TZN fibre ends cannot be cleaved perfectly like normal commercial fibers and unmatched numerical apertures of the high index (~1.82 and ~1.98) mid-IR fibers and the low index (~1.45) normal single mode fiber.

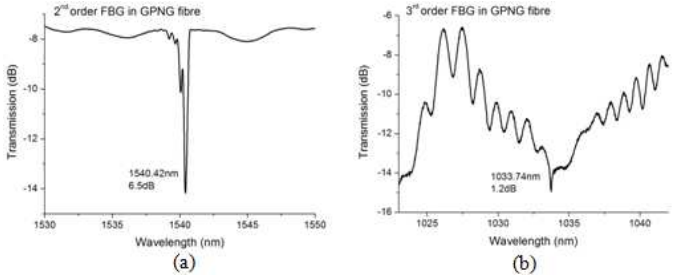

Fig. 5. (a) 2nd and (b) 3rd order FBG resonances of the grating made in GPNG fiber.

Due to higher refractive index and larger size of the core, the passive three-core TZN fiber is actually multimode fiber at ~1694 nm. This is evidenced by the multiple Bragg resonance feature exhibited by the FBGs in all three cores, as shown in Figs. 6(a)-6(c). In the fabrication, the *fs* beam was more focused to the core A, thus we see the grating in core A is the strongest, giving 14.3 dB transmission loss for the lowest mode and the FBG resonances in core B and C achieved a similar strength in an order of ~4 dB. As a prototype device, this result is encouraging and more uniform FBG structures in all three cores should be possible by rotating the three-core fiber and focusing the *fs* beam to the targeted core during the inscription as shown in Fig. 2(b).

#108667 - $15.00 USD Received 11 Mar 2009; revised 9 Apr 2009; accepted 15 Apr 2009; published 22 Apr 2009
(C) 2009 OSA

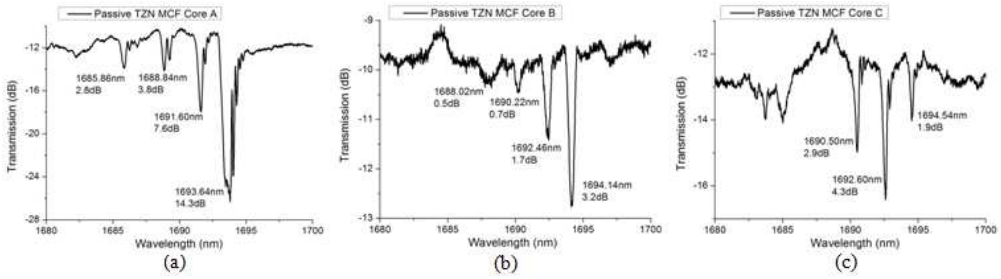

Fig. 6. 2nd order FBG spectra of the passive three-core TZN fiber: (a) core A, (b) core B and (c) core C.

FBG structures were also *fs*-inscribed in the active three-core TZN fiber and the 2nd order FBG spectra of the three cores are shown in Figs. 7(a)-7(c). Here, we only see single resonance in each core indicating the fiber is single mode structure, because its core diameters are smaller than that of passive TZN fiber. The 2nd FBGs are more uniform across the three cores, as we see the strengths of the three resonances at 1678.05 nm, 1676.05 nm and 1676.85 nm in the three cores are 10.6, 5.6 and 6.8 dB, respectively. The refractive index of the TZN fiber core at ~1677 nm can be estimated as ~1.9760.

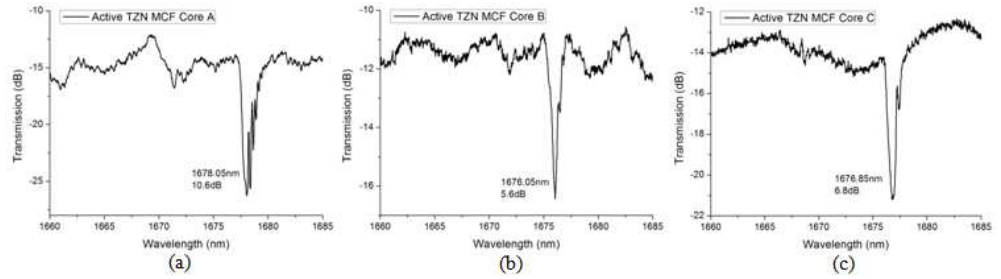

Fig. 7. 2nd order FBG transmission spectra in (a) - (c) the core A-C of the active TZN MCF.

It is noted from Fig. 6 and 7 that some pronounced type of Fabry-Perot structures appear at the longer wavelength side of the Bragg resonances for the TZN fibers, which is different from the normal FBG spectrum. A similar phenomenon was observed for UV-inscribed B/Ge fiber [20] and the simulation suggested that this may be caused by a negative refractive index modulation induced during inscription. This explanation needs to be verified by further experiment in TZN fibers using *fs*-inscription.

5. Thermal responses of the FBGs in germanante and tellurite glass fibers

We then further examined the thermal responses of the *fs*-inscribed FBGs in GPNG and TZN fibers by subjecting the grating fibers to elevating temperatures. The wavelength shifts of the 2nd and 3rd order Bragg resonances of GPNG fiber at 1540 nm and 1033 nm versus the temperature changes from 10 °C to 70 °C with increments of 5 °C are shown in Fig. 8(a). The measured thermal responsivities are 24.71 and 16.80 pm/°C, respectively. Fig. 8(b) shows the thermal responsivities of the active three-core TZN fiber for elevating temperature from 10 °C to 60 °C. The thermal responsivities of cores A - C are measured as 20.21, 18.61 and 19.25 pm/°C, respectively.

The thermal responsivity can be expressed as:

$$\frac{\Delta\lambda}{\Delta T} = \lambda_B \left(\alpha + \frac{\beta}{n_{eff}} \right) \tag{1}$$

#108667 - $15.00 USD Received 11 Mar 2009; revised 9 Apr 2009; accepted 15 Apr 2009; published 22 Apr 2009
(C) 2009 OSA

where $\alpha = \frac{1}{\Lambda}\frac{d\Lambda}{dT}$ is the thermal expansion coefficient, and $\beta = \frac{dn}{dT}$ is the thermo-optic coefficient. For GPNG fiber, α and β given in [21] are 1.09×10^{-5} /°C and 9.0×10^{-6} /°C. Therefore, using the value of refractive index n_{eff}=1.8156, the thermal responsivity for 1540 and 1033 nm can be calculated as 24.43 and 16.39 pm/°C. For TZN fiber, using α=1.86×10^{-5} /°C, β=-1.64×10^{-5} /°C from [22] and n_{eff}=1.9760, we can derive the thermal responsivity for 1676 nm with the value of 17.26 pm/°C. From the above calculation, the experimental thermal responsivities are in good agreement with the theoretical ones.

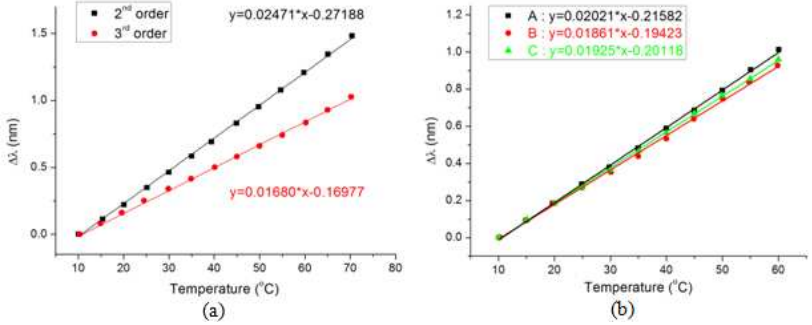

Fig. 8. The wavelength shift of (a) the 2nd and 3rd order resonances of the GPNG fiber at ~1540 and 1033 nm and (b) the 2nd order resonances of the core A-C of the active three-core TZN fiber at ~1677 nm against temperature change.

6. Strain responses of the FBGs in germanante glass fibers

The strain response of the *fs*-inscribed FBGs in GPNG fibers was also examined by applying longitudinal strain to the grating fibers. The strain sensitivity and normalized strain sensitivity of the 2nd order Bragg resonance of GPNG fiber at 1540 nm were measured to be 1.219 pm/με and 0.7912×10^{-6} /με respectively, as shown in Fig. 9(a). These values are consistent with results from strain applied to the fiber configured as a Fabry-Perot interferometer [22]. The optical phase change with strain and the normalized strain sensitivity of GPNG fiber using Fabry-Perot interferometer at 1540nm are 5902×10^{3} rad/m and 0.7910×10^{-6} /με respectively, as shown in Fig. 9(b). The strain responses of germanate glass fiber from the FBG and Fabry-Perot interferometer measurement were consistent with each other with only 0.025% difference in the normalized strain sensitivity.

Strain sensitivity of FBGs can be expressed as:

$$\frac{\Delta\lambda_B}{\varepsilon} = \lambda_B \cdot \left\{1 - \frac{1}{2}\cdot n^2\left[(1-\mu)p_{12} - \mu p_{11}\right]\right\} \tag{2}$$

Optical phase change per unit strain per unit fiber length of the Fabry-Perot interferometer can be express as:

$$\frac{\Delta\phi}{\varepsilon L} = \frac{\Delta\phi}{\Delta L} = \frac{2n\pi}{\lambda}\left\{1 - \frac{1}{2}\cdot n^2\left[(1-\mu)p_{12} - \mu p_{11}\right]\right\} \tag{3}$$

Then the normalized strain sensitivity of the fiber from FBGs and F-P interferometer can be expressed as:

$$\frac{1}{\beta}\cdot\frac{\Delta\phi}{\Delta L} = \frac{1}{\lambda_B}\cdot\frac{\Delta\lambda_B}{\varepsilon} = 1 - \frac{1}{2}\cdot n^2\left[(1-\mu)p_{12} - \mu p_{11}\right] \tag{4}$$

where β is the propagation constant of the mode in the fiber, ε is the longitudinal strain applied to the fiber, μ is Poisson's ratio, p_{11} and p_{12} are the strain-optic coefficients. Using p_{11}=0.225, p_{12}=0.235 and μ=0.232 for germanate glass with composition (mol%) of 30PbO-10Bi_2O_3-60GeO_2 from [23], the strain sensitivity of FBGs and optical phase change with strain of F-P interferometer for 1540nm can be calculated as 1.270 pm/με and 6318×10^{3}

#108667 - $15.00 USD Received 11 Mar 2009; revised 9 Apr 2009; accepted 15 Apr 2009; published 22 Apr 2009
(C) 2009 OSA

rad/m, respectively. The normalized strain sensitivity of germanate glass fiber at 1540nm can be derived with the value of 0.8243×10^{-6} /με, which is 4% higher than the value from experimental measurement. From the above calculation, the experimental strain responses are in good agreement with values calculated using published data for fiber with similar compositions, and the small difference between these experimental and predicted values may be due to the slightly different glass compositions being compared.

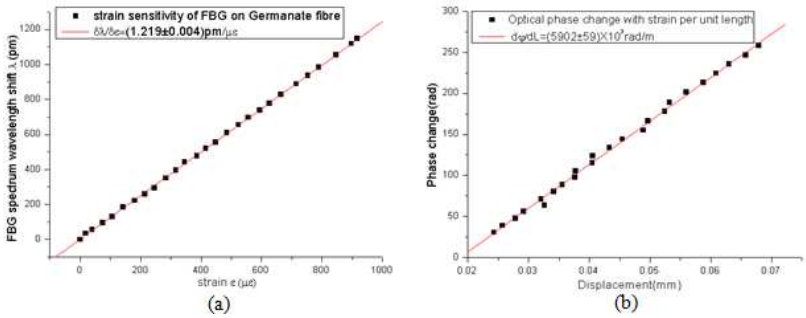

Fig. 9. The strain sensitivity of the 2nd order resonances of (a) the GPNG fiber at ~1540 nm and (b) the optical phase change with strain per unit length of GPNG fiber at ~1540 nm from F-P interferometer.

The strain properties of TZN fiber were also examined using the F-P interferometer method as introduced in [22]. The optical phase change with strain and the normalized strain sensitivity of TZN fiber at 1540nm are 5621×10^{3} rad/m and 0.6787×10^{-6} /με respectively, and the Young's modulus was measured to be 36.7 GPa. Table 1 gives the strain properties of GPNG fiber and TZN fiber from optical measurement and calculation.

From Table 1, we can conclude that the Fabry-Perot experiments show that the phase change per unit length per unit strain ($d\phi/dL$) in tellurite fiber is 4.8% smaller than in the germanate fiber; this proportion is consistent with values calculated using published data for fibers of similar compositions, although the absolute values from experiments are ~6.6% lower than those derived from published properties. Even though tellurite fiber has a higher refractive index, its effect is offset by a larger strain-optic term, which reduces the phase change under strain. However, if we consider the phase change per unit length per unit stress ($\frac{1}{E}\frac{d\phi}{dL}$), the smaller Young's modulus of tellurite fiber compared to germanate leads to a larger response by a factor in the ratio of the measured moduli (51.8 / 36.7) i.e. ~1.4. Hence tellurite fiber would be advantageous as a load sensing element.

Table 1. Strain properties of GPNG and TZN fiber from optical measurement and theoretical calculation

			GPNG	TZN
Optical measurement	F-P cavity $d\phi/dL$ (rad/m)		5902×10^{3}	5621×10^{3}
	FBG $d\lambda_B/\varepsilon$ (pm/με)		1.219	-
	Normalized strain sensitivity (/με)	F-P	0.7910×10^{-6}	0.6787×10^{-6}
		FBG	0.7912×10^{-6}	-
	Young's modulus (GPa)		51.8	36.7
Calculation	μ		0.282 [23]	0.233 [24]
	p_{11}		0.225 [23]	0.0074[24]
	p_{12}		0.235 [23]	0.187 [24]
	$d\phi/dL$ (rad/m)		6318×10^{3}	6018×10^{3}
	$d\lambda_B/\varepsilon$ (pm/με)		1.270	1.090
	Normalized strain sensitivity (/με)		0.8243×10^{-6}	0.7080×10^{-6}
	Young's modulus (GPa)		63.64 [21]	37.15 [25]

#108667 - $15.00 USD Received 11 Mar 2009; revised 9 Apr 2009; accepted 15 Apr 2009; published 22 Apr 2009
(C) 2009 OSA

7. Conclusions

We have for the first time successfully inscribed FBGs in germanate and tellurite glass single- and multi-core fibers using 800 nm femtosecond laser with pulse width of 120 *fs* and a phase mask with the pitch of 1697.33 nm. With peak power intensities in the order of 10^{11} W/cm^2, FBGs in GPNG and TZN fibers were achieved. In the GPNG fiber, the 2nd and 3rd order Bragg resonances are at 1540 and 1033 nm with strengths of 6.5 and 1.2 dB. In the passive and active three-core TZN fibers, the 2nd order resonances at situated at ~1694 and ~1677 nm with strongest peaks exhibiting reflectivities of 14.3 and 10.6 dB, respectively.

In addition, we have characterized thermal responsivities of the FBGs made in two mid-IR fibers. The thermal responsivities of the 2nd and 3rd order Bragg resonances in GPNG fiber were measured as 24.7 and 16.8 pm/°C and that of the 2nd order resonances of the three individual cores of TZN fiber were measured as 20.2, 18.6 and 19.3 pm/°C, respectively. The experimental thermal responsivities are in good agreement with the theoretically calculated ones. The strain and normalized strain sensitivity of 2nd order FBGs in GPNG fiber were also measured as 1.219 pm/με and 0.7192×10^{-6} /με respectively, which is consistent with the value of 0.7190×10^{-6} /με from F-P interferometer measurement. The experimental strain responses are also in good agreement with values calculated using published data for fiber of similar compositions. The strain properties measurement of germanate and tellurite fiber also shows that tellurite fiber would be advantageous as a load sensing element because of the smaller Young's modulus compared to germanate fiber.

Acknowledgments

This work was funded by the UK Engineering and Physical Sciences Research Council (EPSRC). Grant ref. numbers: EP/C515226/1 and EP/C515218/1.

#108667 - $15.00 USD Received 11 Mar 2009; revised 9 Apr 2009; accepted 15 Apr 2009; published 22 Apr 2009
(C) 2009 OSA